Geochemistry Geophysics Geosystems G3

Article
Volume 11, Number 6
2 June 2010
Q06001, doi:10.1029/2010GC003031
ISSN: 1525-2027

Published by AGU and the Geochemical Society

Influence of initial CMB temperature and other parameters on the thermal evolution of Earth's core resulting from thermochemical spherical mantle convection

T. Nakagawa and P. J. Tackley

Institute of Geophysics, ETH Zurich, CH-8092 Zurich, Switzerland (ntakashi@ethz.ch)

[1] Here we present a wide-ranging parameter study of the effects of initial core-mantle boundary (CMB) temperature, concentration of radioactive potassium in the core, and density difference between harzburgite and mid-ocean ridge basalt (MORB) in a coupled spherical model of thermochemical mantle convection and parameterized core heat balance. The initial CMB temperature is expected to be much higher than the solidus temperature of silicates at the base of the mantle. The results indicate that as with previous, purely thermal convection models, the final state of the system is only weakly dependent on initial CMB temperature unless the CMB becomes blanketed by a global layer of dense material. Fully 3-D spherical cases have a very similar core evolution to cases in a 2-D spherical annulus, giving confidence in the applicability of 2-D spherical annulus geometry for modeling Earth's evolution. Obtaining a successful thermal evolution, in the sense of obtaining the correct present-day inner core size and maintaining a geodynamo over geological time, is helped by the accumulation of piles of dense material at the CMB (subducted MORB in the present calculations) and a concentration of radiogenic K in the core in the range 400–800 ppm. The present-day CMB heat flow is predicted to be around 9 TW. While this is lower than estimates based on calculating temperature gradients in regions where the postperovskite transition is seismically imaged, these tend to be areas of higher than average heat flux and thus likely overestimate the global heat flow.

Components: 7500 words, 12 figures, 4 tables.

Keywords: CMB temperature; CMB heat flow; thermal evolution; early Earth.

Index Terms: 8125 Tectonophysics: Evolution of the Earth (0325); 8130 Tectonophysics: Heat generation and transport.

Received 6 January 2010; **Revised** 19 April 2010; **Accepted** 22 April 2010; **Published** 2 June 2010.

Nakagawa, T., and P. J. Tackley (2010), Influence of initial CMB temperature and other parameters on the thermal evolution of Earth's core resulting from thermochemical spherical mantle convection, *Geochem. Geophys. Geosyst.*, *11*, Q06001, doi:10.1029/2010GC003031.

1. Introduction

[2] Understanding the thermal evolution of the Earth's core is challenging because it is difficult to extract enough heat from the core over geological time to drive the geodynamo while not growing the inner core larger than its present size [e.g., *Labrosse*, 2003; *Nimmo et al.*, 2004]. Mantle convection determines the heat flux across the core-mantle boundary (CMB). Our previous studies of the thermal evolution of the Earth's core using global thermochemical mantle convection modeling coupled to a parameterized core heat balance [*Nakagawa and Tackley*, 2004a, 2005a] suggested that it is necessary

to have a partial layer of chemically dense material above the CMB in order to reduce CMB heat flux sufficiently to prevent the inner core becoming too large (compared to Earth's): isochemical convection resulted in a large CMB heat flux that results in a too-large inner core. Possible candidates for such dense material are subducted mid-ocean ridge basalt (MORB) [*Christensen and Hofmann*, 1994] or material that formed from the initial differentiation or soon after [e.g., *Solomatov*, 2000; *Boyet and Carlson*, 2005; *Labrosse et al.*, 2007].

[3] In our previous studies [*Nakagawa and Tackley*, 2004a, 2005a], we considered only one initial CMB temperature, which was the solidus temperature of peridotite at the CMB [*Boehler*, 2000], whereas it is generally thought that the CMB may have started off as much as 2000 K hotter than this after core formation [*Stevenson*, 1990]. Based on simple isochemical mantle thermal evolution models, this might not be expected to have a significant effect on the present-day mantle because it "forgets" its initial condition within ~1 Gyr [e.g., *Sharpe and Peltier*, 1978]. For thermochemical convection, however, the situation needs to be evaluated, because different early temperatures could influence the formation of compositional anomalies, which then have a long-term effect on subsequent evolution. For example, higher temperature could cause more melting and crustal production, hence a thicker layer of segregated crust above the CMB; alternatively a higher temperature drop across the lower thermal boundary layer would make compositional layering less stable. Other limitations of our previous core evolution studies are that they did not include the post-perovskite phase [*Murakami et al.*, 2004; *Oganov and Ono*, 2004], which was subsequently shown to have some effect on deep mantle dynamics and core heat flow [*Nakagawa and Tackley*, 2004b, 2005b, 2006; *Tackley et al.*, 2007], and that they were performed in a two-dimensional (2-D) cylindrical geometry.

[4] Here, we thus present thermochemical evolution models that investigate the sensitivity of the model evolution to initial CMB temperatures of up to ~6000 K using a 2-D spherical annulus geometry (with some cases checked in a 3-D spherical shell), and including the postperovskite phase transition in addition to the other previously included major phase transitions. The fraction of MORB material is reduced to 20% (compared to 30% in previous models) in accordance with mantle bulk composition [*Xu et al.*, 2008]. We systematically study the sensitivity of the final (present-day) state to initial CMB temperature, density anomaly of MORB in the deep mantle, and concentration of radiogenic potassium in the core.

[5] If temperatures near the CMB were substantially hotter than the mantle solidus temperature then widespread melting would have been present; indeed, partial melting may still exist today in the form of ultralow-velocity zones (ULVZs), which have been extensively probed by seismological data [e.g., *Williams and Garnero*, 1996; *Williams et al.*, 1998]; a partial melt explanation is feasible if melt is of similar or slightly higher density than the solid matrix [*Stixrude and Karki*, 2005; *Hernlund and Tackley*, 2007]. This scenario was termed the "Basal Magma Ocean" (BMO) hypothesis by [*Labrosse et al.*, 2007], who examined its various geochemical and geophysical consequences. The calculations presented here, while not attempting to treat the chemical and physical effects of melting at the base of the mantle, can give some clues as to the longevity of such a magmatic region.

2. Model

[6] A coupled model, in which a 2-D or 3-D thermochemical mantle convection calculation is coupled to a parameterized core heat balance, is used here. The model is very similar to that in our previous papers on the topic [*Nakagawa and Tackley*, 2004a, 2005a], for which the reader is referred for full details. To summarize: The compressible truncated anelastic approximation is assumed, with depth-dependent material properties except for viscosity, which is dependent on both temperature and depth, varying by six orders of magnitude with temperature, two orders of magnitude with depth plus a factor of ten viscosity jump at 660 km depth, and undergoes plastic yielding to mobilize the lithosphere, with a constant yield stress of 120 MPa. Truncating the anelastic liquid approximation causes a minor error in energy conservation [*Leng and Zhong*, 2008; *King et al.*, 2010] but this is small compared to the general uncertainties and approximations in the model.

[7] We focus on the differences to our previous models. The thermochemical convection model is now in spherical (rather than cylindrical) geometry using StagYY [*Tackley*, 2008]. The geometry used for most calculations is a 2-D spherical annulus [*Hernlund and Tackley*, 2008], with two cases also calculated in a full 3-D spherical shell. All major phase transitions in the olivine and pyroxene-garnet systems (olivine-spinel-perovskite-postperovskite and pyroxene-garnet-perovskite-postperovsite, respec-

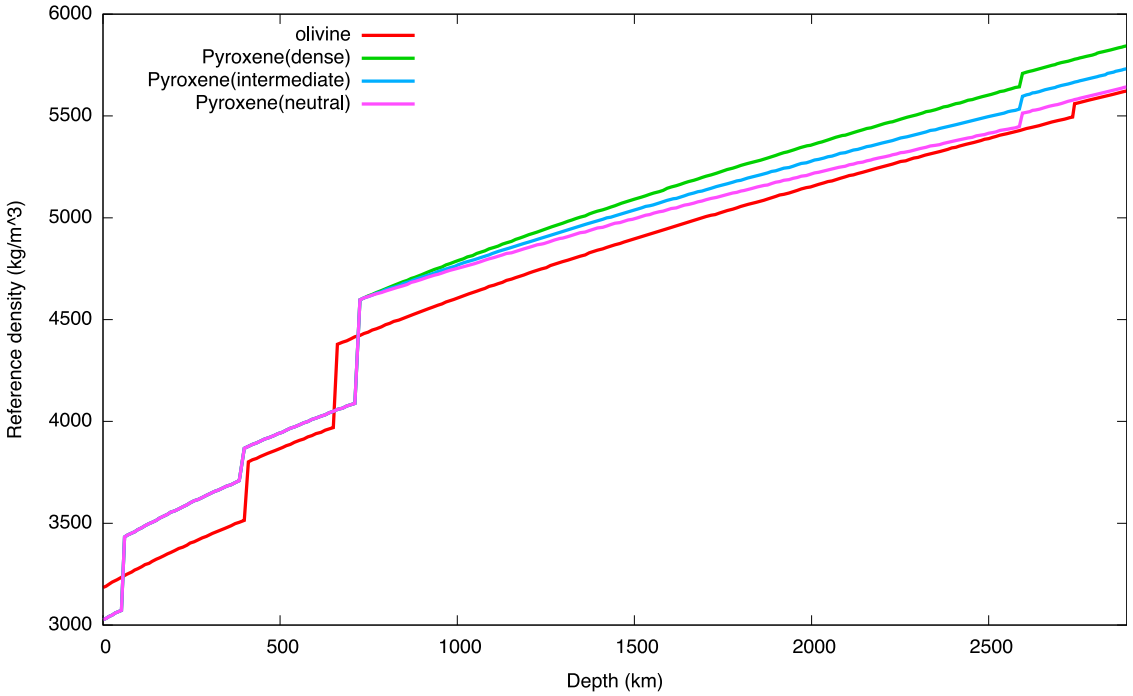

Figure 1. Reference density profile along the 1600 K adiabat. Three compressibilities are assumed for the pyroxene/garnet component in the lower mantle, which might be related to the alumina component in the lower mantle minerals [e.g., *Weidner and Wang*, 1998], and lead to neutral, intermediate, or dense MORB at the CMB.

tively) are included, as shown by the density jumps in Figure 1. The mantle is assumed to be a mechanical mixture of harzburgite and MORB, with MORB consisting of pure pyroxene-garnet and harzburgite consisting of 3/4 olivine and 1/4 pyroxene-garnet. There is some uncertainty in the density of the MORB assemblage in the deep mantle, due to different compressibilities of different minerals [e.g., *Kesson et al.*, 1998; *Ono et al.*, 2001; *Hirose et al.*, 2005]. By adjusting the compressibilty of the pyroxene-garnet mineralogy in the lower mantle, the density difference between the olivine system and the pyroxene-garnet system at CMB pressures is either 0% (neutral), 1.8% (intermediate) or 3.6% (dense) (see Figure 1). This corresponds to a density difference between MORB and harzburgite of up to 2.7%, and between MORB and pyrolite (20% MORB and 80% harzburgite) of up to 2.16%. Since the postperovskite phase transition for MORB may occur at a shallower depth than that for the olivine system [*Hirose*, 2006; *Ohta et al.*, 2008], the postperovskite phase transition at a temperature of 3000 K is assumed to take place at 2600 km and 2740 km depth for pyroxene and olivine, respectively. A numerical resolution of 512 × 128 cells for 2-D spherical annulus and 64 × 192 × 64 × 2 (equivalent to 256 (longitude) × 128 (latitude) × 64 (radial)) cells for 3-D spherical shell is used, with an average of 15 tracers/cell to track chemical composition and melt fraction. The detailed formulation of the viscosity law and density profiles are given by *Nakagawa and Tackley* [2005a]. All physical parameters for mantle and core models are listed in Tables 1 and 2, respectively.

[8] The initial temperature structure in the mantle is adiabatic with a potential temperature of 1650 K, plus thin thermal boundary layers at the top and bottom, and small random perturbation. The chemical composition, which represents the MORB fraction, is initially uniform at C = 0.2, which is consistent with the amount of MORB that can exist in the pyrolite composition [*Xu et al.*, 2008]. Melt-induced differentiation generates the crust, which when subducted, generates compositionally heterogeneous structures. A total of 48 cases are presented here, featuring four initial CMB temperatures ranging from 4412 K to 5912 K, four concentrations of radioactive potassium in the core and three density variations between olivine and pyroxene. All cases are run for 4.5 Ga.

3. Results

3.1. Thermochemical Structures

[9] The time evolution of thermochemical structures for two representative cases is shown in Figures 2

Table 1. Mantle Model Physical Parameters[a]

Symbol	Meaning	Nondimensional Value	Dimensional Value
Ra_0	Rayleigh number	10^7	N/A
η_0	Reference viscosity	1	1.4×10^{22} Pa s
$\Delta\eta$	Viscosity jump at 660 km	10	N/A
σ_b	Yield stress at surface	1×10^5	117 MPa
σ_d	Yield stress gradient	4×10^5	162.4 Pa m^{-1}
ρ_0	Reference (surface) density	1	3300 kg m^{-3}
g	Gravity	1	9.8 m s^{-2}
α_0	Ref. (surface) thermal expan.	1	5×10^{-5} K^{-1}
κ_0	Ref. (surface) thermal diff.	1	7×10^{-7} m^2 s^{-1}
ΔT_{sa}	Temperature scale	1	2500 K
T_s	Surface Temperature	0.12	300 K
L_m	Latent Heat	0.2	6.25×10^5 J kg^{-1}
τ	Half-life	0.00642	2.43 Gyr
H	Internal heating rate at the present time	20.63	5.6×10^{-12} W/kg

[a] $Ra_0 = \rho_0 g \alpha_0 \Delta T_{sa} d^3 / \kappa_0 \eta_0$.

and 3. Figure 2 shows the time evolution of the case with an initial T_{CMB} of 4412 K, intermediate MORB density anomaly and no K in the core. Small-scale dense piles covering part of the CMB start accumulating above the CMB 3.6 Ga before present, then become larger-scale with time. A case with identical parameters except for a T_{CMB}^{init} of 5912 K is shown in Figure 3. The main features are very similar to those of the case with the lower initial CMB temperature (Figure 2) except that there is more vigorous activity early in the evolution, with more differentiation taking place and larger and more vigorous plumes. In addition, at early times compositionally dense piles are less stable above the CMB that in the lower initial CMB temperature case (Figure 2).

[10] Figure 4 shows compositional structures at the present day (after 4.5 Gyr of evolution) for cases with different MORB density contrast but the same initial T_{CMB} of either 4412 K (Figures 4a–4c) or 5912 K (Figures 4d–4f). With neutral density contrast (Figures 4a and 4d), subducted MORB does not form a layer at the CMB, while with intermediate density contrast (Figures 4b and 4e) it forms discontinuous piles and at the full density contrast (Figures 4c and 4f) it forms an almost global layer, with slab-like downwellings pushing it aside in two places. Thus, large-scale high-temperature regions above the CMB are found for both intermediate and large density contrasts. The fields for cases with initial T_{CMB} = 5912 K (Figures 4d–4f) look remarkably similar in character to those with the lower initial T_{CMB} (Figures 4a–4c). Slight differences are that in the dense MORB case the layer looks slightly more extensive, while in the intermediate density case the piles have a shorter length scale. This implies that by 4.5 Ga, the system has lost most memory of its initial condition. The general character of thermochemical structures in these cases with yielding-induced plate-like behavior is similar to that in other studies with force-balanced plates [e.g., *Brandenburg et al.*, 2008] implying that the details of the plate treatment are not important.

3.2. Time Diagnostics: Core Evolution

[11] Figures 5 and 6 show the time evolution of CMB temperature, CMB heat flux, inner core size and ohmic dissipation for various initial CMB temperatures and the intermediate MORB density

Table 2. Physical Parameters for the Core Heat Balance[a]

Symbol	Meaning	Value
r_{CMB}	Radius of the core	3486 km
ρ_c	Init. density of core	12300 kg m^{-3}
ρ_{iron}	Density of pure iron	12700 kg m^{-3}
ρ_{li}	Density of light elements	4950 kg m^{-3}
$\Delta\rho_{IC}$	Density difference	400 kg m^{-3}
ΔS	Entropy change	118 J kg^{-1} K^{-1}
$C_l(t = 0)$	Init. Cont. of light elements	0.035
C_c	Heat capacity of the core	800 J kg^{-1} K^{-1}
$T_L(r = 0, C_l(t = 0))$	Melting T. at the center	5300 K

[a] The value of entropy change is taken from *Labrosse* [2003]. The melting temperature at the Earth's center is taken from *Lister* [2003]. All other values are taken from *Buffett et al.* [1996].

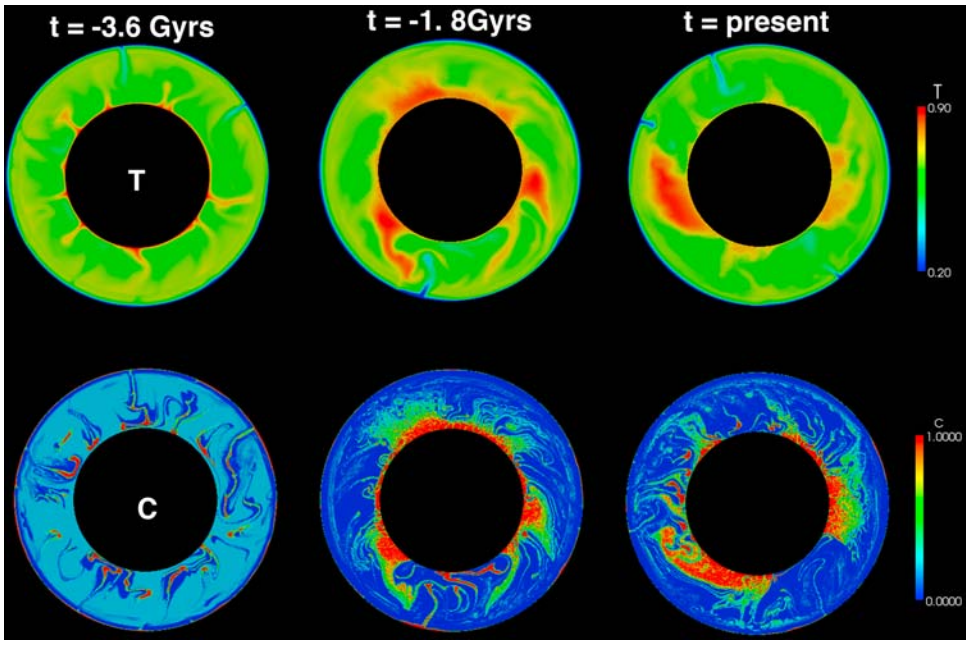

Figure 2. Time evolution of (top) temperature and (bottom) composition for the intermediate buoyancy case of an initial CMB temperature of 4412 K with 0 ppm core potassium.

contrast, with Figure 5 showing cases with 0 ppm core potassium and Figure 6 showing cases with 800 ppm core potassium. As expected, at early times the CMB heat flux is large and the CMB temperature drops rapidly. In both Figures 5 and 6, it is clear that the final state of the system, for example in terms of CMB heat flux, temperature and inner core size, is only weakly dependent on the initial condition, which has a strong influence on only approximately the first half of the model history as well as the age of the inner core. With 800 ppm potassium in the core (Figure 6), the core remains hot enough that the inner core has barely started to grow by the present day, while with no potassium in the core, the inner

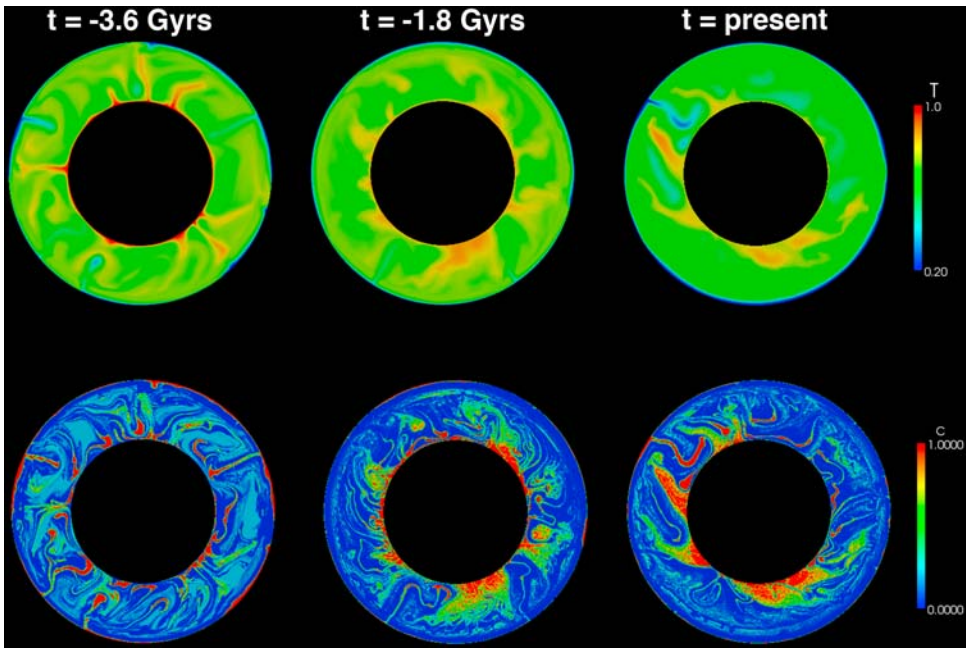

Figure 3. Same as Figure 2 but with higher initial CMB temperature that is 5912 K.

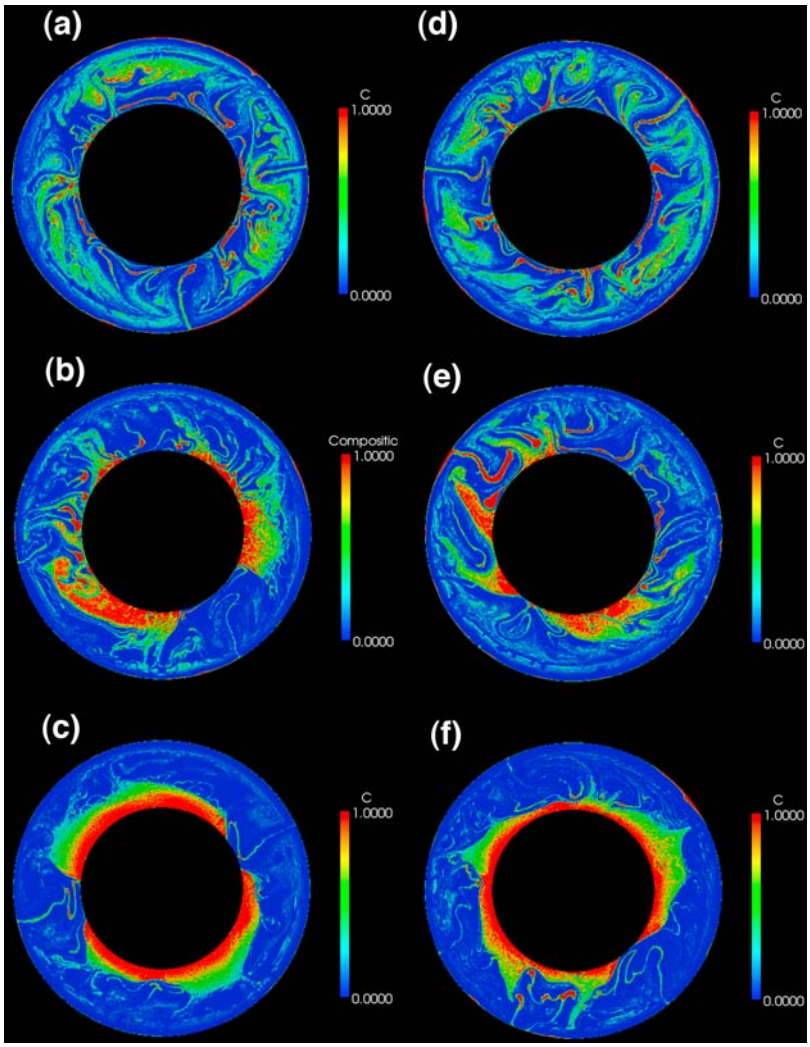

Figure 4. Chemical structures for three compressibilties at the final time step, with an initial CMB temperature of 4412 K ((a) neutral, (b) intermediate, and (c) dense) and 5912 K ((d) neutral, (e) intermediate, and (f) dense) with 0 ppm core potassium.

core grows too large (the actual size is 1220 km), with small differences between cases with different initial T_{CMB}. In all cases, ohmic dissipation is positive for the entire evolution, meaning that a geodynamo is possible for the entire history.

[12] When MORB is substantially dense at the CMB and there is no core potassium (Figure 7), the final state becomes more dependent on initial CMB temperature, with a difference of about 400 K in final CMB temperature. This leads to an inner core size that varies from zero to 1300 km depending on initial T_{CMB}. Unfortunately, in all of these cases the dense layer blankets the core so effectively that the heat flux drops too low for a geodynamo to be sustained, as indicated by zero ohmic dissipation toward the end of the calculations; therefore these are not considered to be viable histories for Earth.

[13] When MORB is neutrally dense at the CMB and there is no core potassium (Figure 8), the evolution is somewhat similar to the cases with intermediate density MORB but the CMB heat flux is higher, which results in a lower final CMB temperature and a larger inner core. Therefore, as found in our previous studies, partial layering at the CMB is helpful in preventing the inner core from becoming too large. The final T_{CMB} varies by only about 150 K for a 1500 K variation in initial T_{CMB}.

3.3. Regime Diagrams, Analytical Fit, and "Best Fit" Models

[14] In order to quantify clearly the dependence of outputs (final inner core size, T_{CMB} and ohmic dissipation) on input parameters (initial T_{CMB}, ppm K

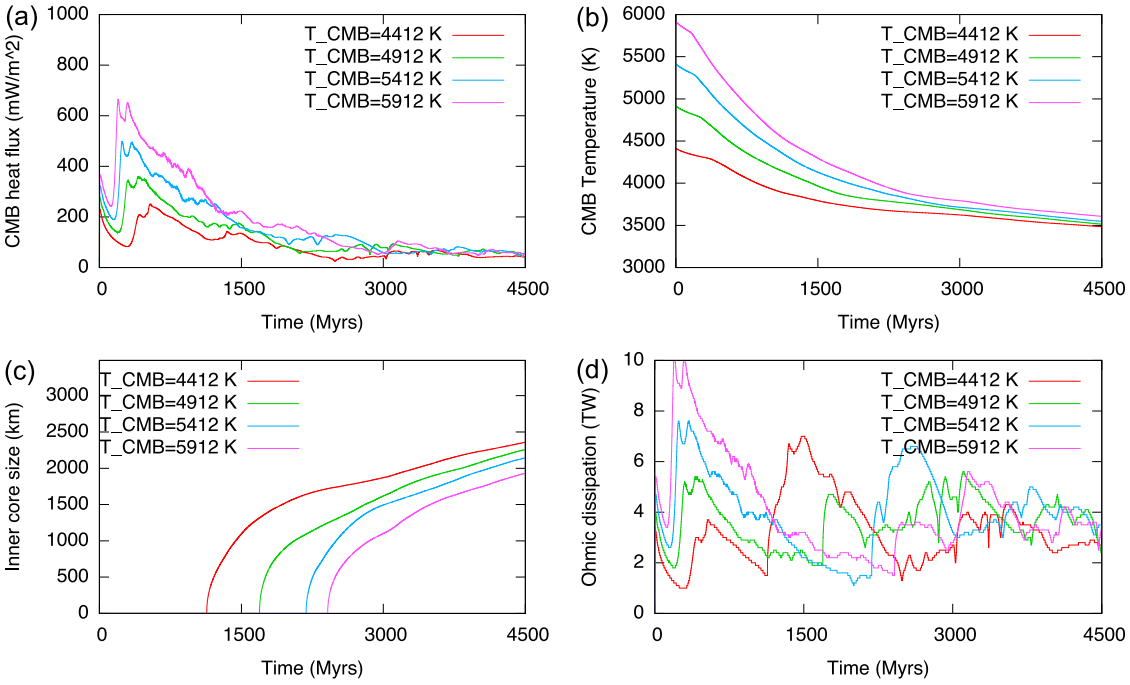

Figure 5. Time diagnostics of (a) CMB heat flux, (b) CMB temperature, (c) inner core size, and (d) ohmic dissipation for 0 ppm core potassium and an intermediate MORB density contrast.

and MORB density anomaly) and to identify which model or models best fit the constraints of positive ohmic dissipation over the history and reasonable final inner core size, all 48 cases are plot on three regime diagrams, with axes of final inner core size and magnetic dissipation averaged over the last 2 Ga of the evolution (Figure 9). The three plots show the same points, but they are colored in different ways in

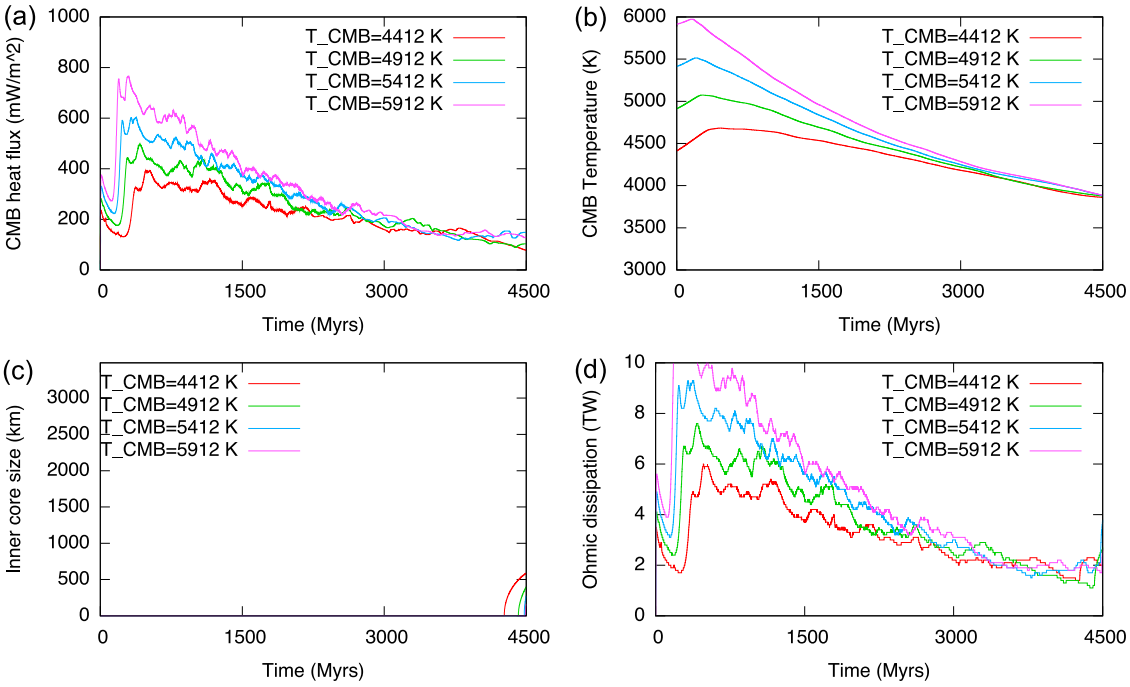

Figure 6. Same as Figure 5 but with 800 ppm core potassium.

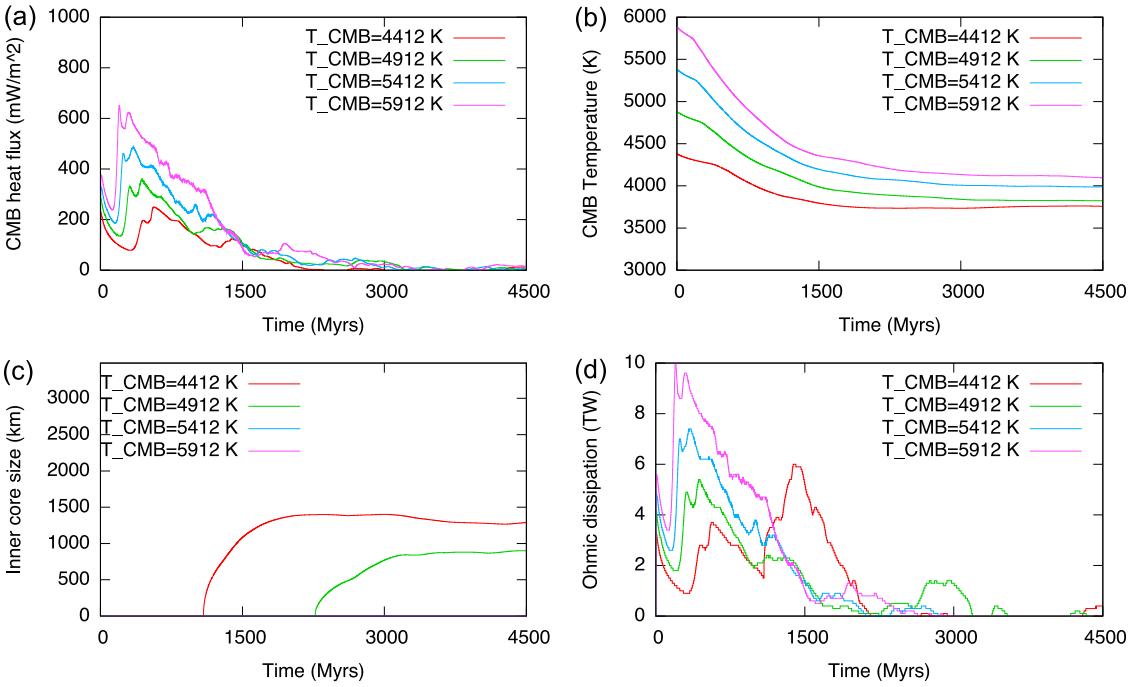

Figure 7. Same as Figure 5 but with dense MORB.

each plot in order to show the dependence on different input parameters. These plots show a clear dependence of ohmic dissipation and inner core size on K concentration (Figure 9b) and MORB density anomaly (Figure 9c) but only a small dependence on initial T_{CMB} (Figure 9a).

[15] These are quantitatively analyzed by assuming that inner core size (r_{IC}), magnetic dissipation (Φ_m) and final CMB temperature (T_{CMB}^{final}) are linearly dependent on initial CMB temperature (T_{CMB}^{init}), amount of radioactive potassium (C_K) and density difference between MORB and harzburgite

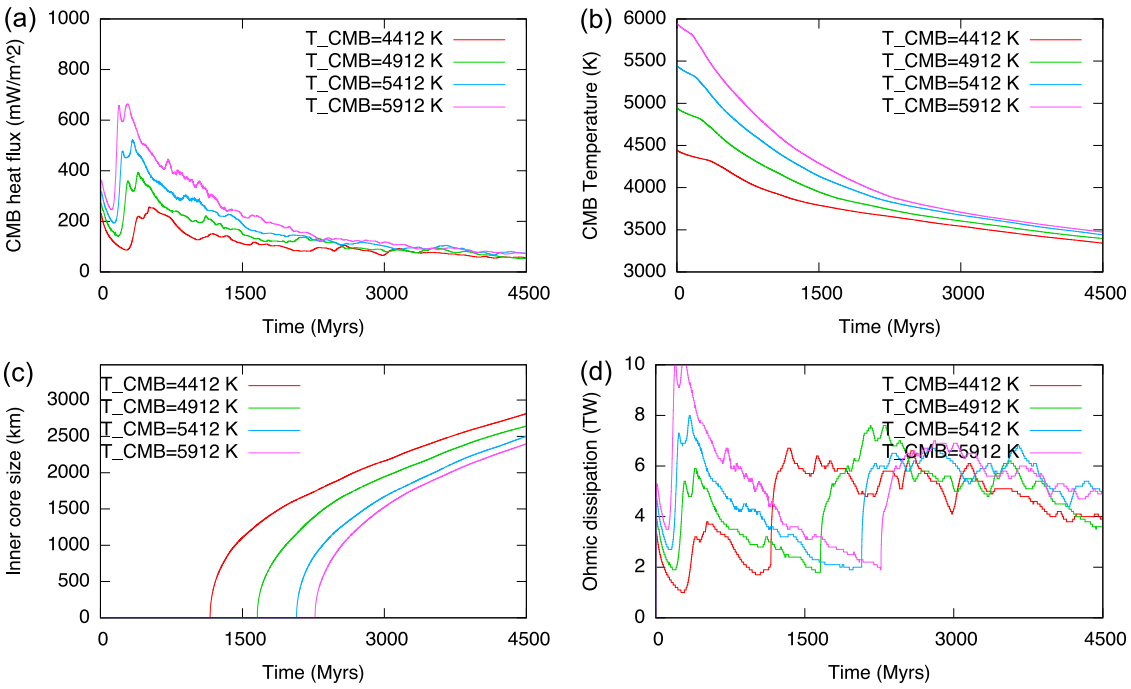

Figure 8. Same as Figure 5 but with neutral MORB density.

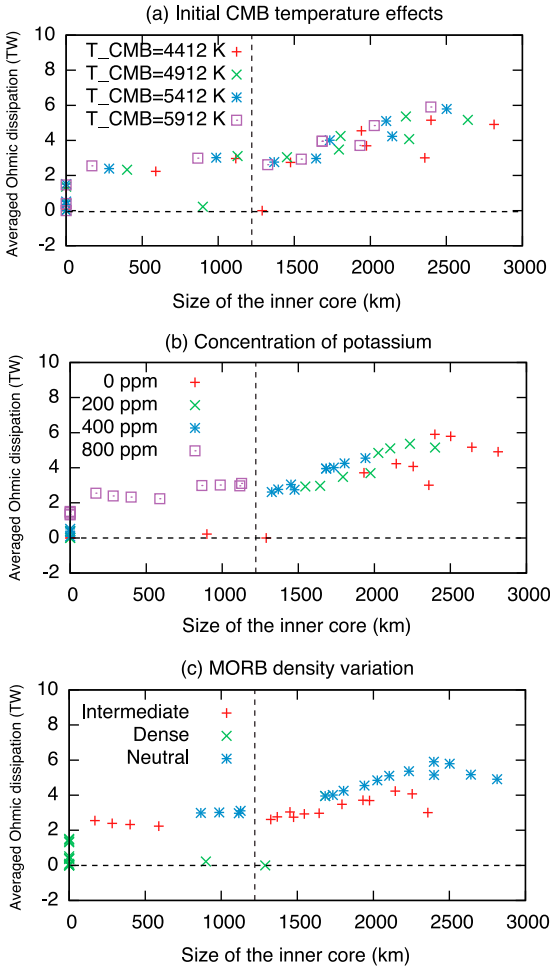

Figure 9. Regime diagrams showing the final inner core radius and ohmic dissipation (averaged over the last 2 Ga) for the 48 different cases. The correct inner core radius is indicated by the vertical dashed line. Coloring shows (a) initial CMB temperature, (b) amount of potassium in the core, and (c) compressibility in the lower mantle.

$(\Delta\rho_m/\rho_{CMB})$ and performing a least squares fit to find the scaling factors, i.e., assuming that

$$r_{IC} = a_{IC} + b_{IC}T^{init}_{CMB} + c_{IC}C_K + d_{IC}\left(\frac{\Delta\rho_m}{\rho_{CMB}}\right)$$
$$\Phi_m = a_{md} + b_{md}T^{init}_{CMB} + c_{md}C_K + d_{md}\left(\frac{\Delta\rho_m}{\rho_{CMB}}\right) \quad (1)$$
$$T^{final}_{CMB} = a_{CMB} + b_{CMB}T^{init}_{CMB} + c_{CMB}C_K + d_{CMB}\left(\frac{\Delta\rho_m}{\rho_{CMB}}\right)$$

where a, b, c and d are coefficients determined by least squares fitting in four-dimensional space. Table 3 lists all coefficients and the remaining variance and standard deviation of each relationship with variance reduction from the variance obtained from raw data plotted in Figure 9. For all three outputs, variance reductions of around 80% are obtained, which means that the variance of the residual (i.e., data minus fit) is about 20% of the data variance. In order to check which input parameters are most influential, calculations of the variance when dropping two terms on the right hand side of the fitting equations (e.g., if focusing the initial CMB temperature, the other two inputs are dropped) are shown in Table 4. These show that the MORB density anomaly is the most important parameter controlling inner core size, magnetic dissipation and final CMB temperature. Since the heat flux across the CMB is the most important factor for understanding the thermal evolution of Earth's core [e.g., *Buffett*, 2002; *Labrosse*, 2003], MORB density anomaly works by determining the formation of dense piles, dense layer and/or no compositional layer that can buffer the heat flux across the CMB. Indeed, for magnetic dissipation it is the only important parameter. Core potassium content has a significant influence on final inner core size and CMB temperature, while initial CMB temperature has a very minimal influence. It is noted that the spatial variations of CMB heat flux may also influence the geodynamo [e.g., *Aubert et al.*, 2008].

[16] Several best fitting models can be identified from Figure 9, as models with close to the correct inner core size and nonzero ohmic dissipation. The four best fitting models have (T^{init}_{CMB}, $\Delta\rho_m/\rho_{CMB}$, C_K) of (4412 K, neutral, 800 ppm), (4912 K, neutral, 800 ppm), (5912 K, intermediate, 400 ppm) and (5412 K, intermediate, 400 ppm). Therefore, any initial CMB temperature is possible; the essential properties are relatively low MORB density contrast and high core potassium concentration.

[17] Figure 10 shows time evolutions for two of the best fitting models: (5912 K, intermediate, 400 ppm) and (4912 K, neutral, 800 ppm), as well as, for comparison, the (4412 K, dense, 0 ppm) case that fits the core size constraint but not the dynamo

Table 3. Coefficients of Equation (1) Obtained by Linear Least Squares Fitting[a]

	a	b	c	d	Variance Reduction (%)
Inner core size (nondimensional)	0.9452	-4.0226×10^{-5}	−449.6472	−13.2815	79.9
Magnetic dissipation	3.5034	2.7450×10^{-4}	−911.9251	−104.8613	76.3
Final T_{CMB}	3203.4	3.5319×10^{-2}	456517.6	14397.33	82.2

[a]Variance reductions are one minus the ratio of the variance of the residual (i.e., data − fit) to the variance of the raw data.

Table 4. Variance Reductions of Fits Using Only One Input Parameter[a]

	Initial T_{CMB}	Core K	MORB Density
Inner core size	0.3	25.3	53.9
Magnetic dissipation	1.5	2.2	73.3
Final T_{CMB}	0.2	23.8	57.9

[a]Unit is percent.

constraint because core heat flux falls to subcritical. In the two best fitting cases, inner core growth occurs quite late, starting 0.5–1 Ga ago, with the CMB heat flow decaying steadily throughout the history (after an initial transient). In the case with dense MORB, the inner core grows early but remains at an approximately constant size, due to the CMB heat flow falling to ~zero after about 2 Ga, which is caused by blanketing of the core by crust that is enriched in heat-producing elements.

[18] The CMB temperature also decreases with time, except in the later evolution of the (4412, dense, 0 ppm) case where it slightly increases with time because of blanketing of the core by MORB as described above. In contrast, volume-averaged mantle temperature initially increases with time due to high internal heating, but it then buffered by melting, decreasing only slowly in the later part of model evolution, and is quite insensitive to initial CMB temperature, MORB density anomaly, core

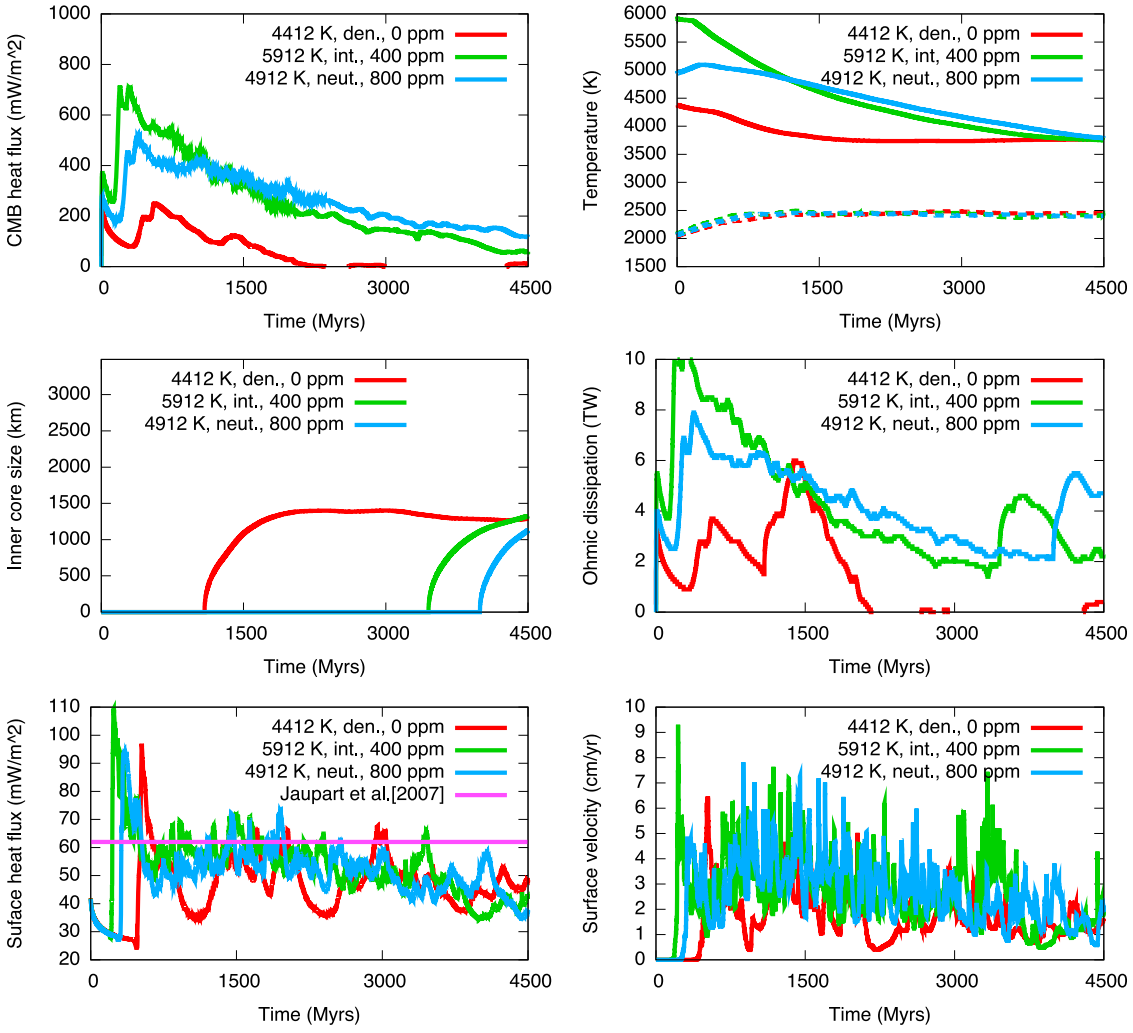

Figure 10. Time evolutions of two best fit models, (1) initial T_{CMB} = 5912 K, intermediate MORB density, and 400 ppm potassium and (2) initial T_{CMB} = 4912 K, neutral MORB density, and 800 ppm potassium, and a model that fits the final inner core size but with a failing geodynamo (initial T_{CMB} = 4412 K, dense MORB, and 0 ppm potassium). For the temperature plot, solid lines indicate the CMB temperature, and dashed lines indicate the volume-averaged mantle temperature.

radioactivity and probably, initial mantle temperature, although the latter needs to be verified.

[19] The magnetic dissipation in the best fitting models is in the range 2.5–3.0 TW, which is larger than theoretical estimates of 0.1 TW to 0.5 TW [*Buffett*, 2002; *Labrosse*, 2003]. This means that a lower CMB heat flux would also give a successful evolution, but such a case does not occur in the parameter range investigated here. The present-day CMB heat flow for the best fitting models is approximately 9 TW, which is close to what was found in our previous study (8.5 TW) [*Nakagawa and Tackley*, 2005a]. This global heat flow is lower than estimates of around 15 TW obtained by estimating the temperature gradient from seismically imaged crossings of the postperovskite phase boundary [*Hernlund et al.*, 2005; *Lay et al.*, 2006; *van der Hilst et al.*, 2007]; however, these tend to be in colder than average areas where the heat flux is higher than the global average.

[20] The time evolution of surface heat flux and velocity for these three models is also shown in Figure 10. The present-day model heat flux ranges from 35 to 50 mW/m^2, which is a factor of 1.5 to 2 lower than recent estimates of Earth's present-day heat flux [*Jaupart et al.*, 2007], while present-day surface velocities range from 1.5 to 4 cm/yr, lower than or comparable to the present-day RMS poloidal plate velocity of 3 cm/yr [*Lithgow-Bertelloni et al.*, 1993]. This reflects a long-standing paradox: understanding why Earth's present-day heat flux is so high compared to the radiogenic heat input (i.e., why the Urey number is low) [*Jaupart et al.*, 2007]. The present results do not provide a solution to this problem, but we note the large fluctuations in surface heat flux and velocity, which may reflect variations in convective cell size [*Grigné et al.*, 2005] and become even larger in the presence of supercontinent cycles [*Grigné et al.*, 2007] and/or plate reorganizations [*Gait and Lowman*, 2007; *Gait et al.*, 2008], suggesting the solution that Earth's present-day heat flux is not representative of the long-term secular trend but rather a high fluctuation. Present-day core size is a constraint on the integrated evolution of the system, whereas present-day surface heat flux and velocity are instantaneous observations whose robustness is uncertain.

3.4. Three-Dimensional Spherical Comparison

[21] In order to check whether dimensionality makes a difference to the essential findings, two of the 2-D spherical annulus models are run in fully 3-D spherical geometry: one of the best fit models with (T^{init}_{CMB}, $\Delta\rho_m/\rho_{CMB}$, C_K) = (5912 K, intermediate, 400 ppm) and the case with (4412 K, dense, 0 ppm), which fits the final inner core size but has zero CMB heat flux through the last part of the evolution. Figure 11 compares the thermochemical structures of 2-D and 3-D models, while Figure 12 compares the time evolution. The isosurfaces of residual temperature (Figures 11c and 11g) indicate that the downwellings are linear features, consistent with the projection of the 2-D downwellings into a third dimension, while isosurfaces of composition (Figures 11d and 11h) indicate an intermittent layer for the intermediate density contrast case and a global layer for the high density contrast case, consistent with the 2-D cases. The time evolution graphs (Figure 12) indicate a surprisingly close correspondence between cases in the different dimensionalities, the only difference being a slightly later onset of inner core formation in the 3-D high density contrast case. These comparisons show that 2-D spherical annulus geometry is a good 2-D approximation to 3-D spherical geometry, and that the core evolutions obtained from 2-D spherical annulus models are representative of what would be obtained in a 3-D spherical shell. This is consistent with the tests performed by *Hernlund and Tackley* [2008], which also showed that the rescaled radius cylindrical geometry [*van Keken*, 2001] used in our previous papers [e.g., *Nakagawa and Tackley*, 2004a, 2005a] gives similar heat fluxes.

4. Discussion and Conclusions

4.1. Insensitivity to Initial Conditions

[22] Several parameterized thermal evolution models of Earth's mantle have indicated that the solution converges to almost the same state regardless of the initial mantle and core temperatures [e.g., *Sharpe and Peltier*, 1978; *Schubert*, 1979]. Our modeling results of thermochemical convection with melt-induced differentiation display the same phenomenon, with (for a given C_K and MORB density) the final CMB temperatures being within 150 K of each other, even though initial CMB temperature varies by 1500 K. Although cases with a higher initial CMB temperature display more vigorous convection and differentiation early on, the larger temperature difference across the lower thermal boundary layer mitigates against a stronger basal layer building up. The exception to this is the cases with relatively dense MORB in the deep mantle, in which a thick layer accumulates above the CMB, resulting in close to zero CMB heat flux after about 2 Ga and a

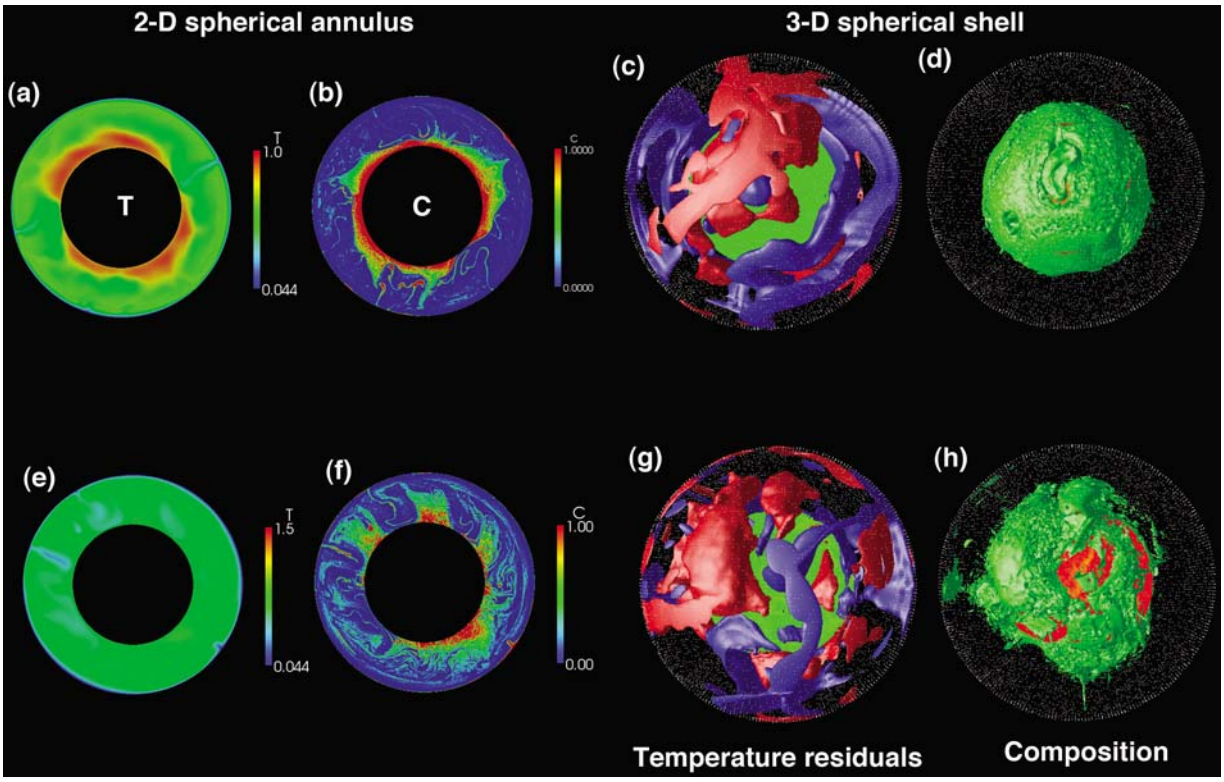

Figure 11. Comparison of thermochemical structures between (a, b, e, and f) 2-D spherical annulus and (c, d, g, and h) 3-D spherical shell for one best fit model (initial T_{CMB} = 5912 K, intermediate MORB density, and 400 ppm potassium) and a model with the correct final inner core size but a failing geodynamo (initial T_{CMB} = 4412 K, dense MORB, and 0 ppm potassium). In the 3-D cases, the red and blue isosurfaces indicate +250 K and −250 K temperature anomalies compared to the geotherm, while the green isosurfaces show 75% basalt fraction.

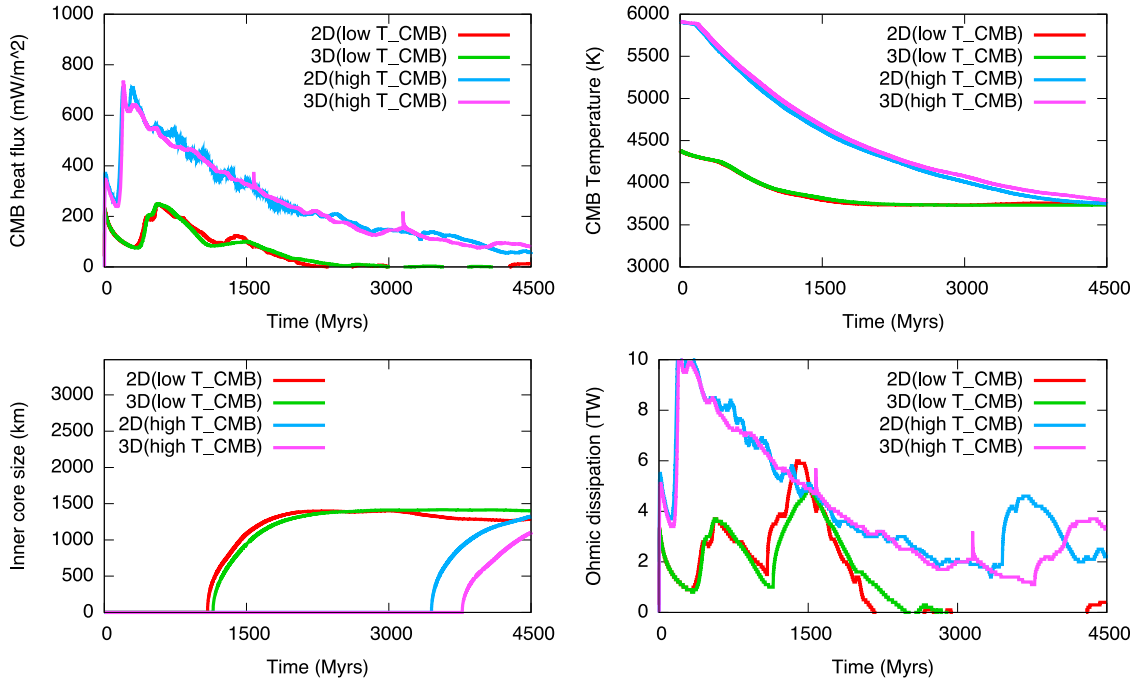

Figure 12. Time diagnostics comparing equivalent 2-D spherical annulus and 3-D spherical shell cases as in Figure 11.

final CMB temperature range of about 400 K. The results are also expected to be insensitive to initial mantle temperature because early on the high internal heating rapidly heats the mantle until the temperature is buffered by melting; thus our use of a present-day initial adiabat of 1650 K [*Jaupart et al.*, 2007] is not expected to make a difference, although this should be verified in the future.

4.2. Effects of the Postperovskite Phase Transition

[23] A new feature in this study, compared to our previous core cooling studies, is the postperovskite phase transition. Comparing the present results to ones without the postperovskite phase transition [*Nakagawa and Tackley*, 2005a], the best fit model parameters appear to be slightly different: in our previous study a low initial CMB temperature coupled with intermediate MORB density and low (100 ppm) K concentration was successful, whereas substantially higher K is required here. However, it is quite likely that the difference in geometry might explain a large part of this, so no firm conclusions can be drawn without further study.

[24] Several studies have estimated the heat flow across the CMB using the relationship between geotherm and seismically observed postperovskite phase boundary [*Hernlund et al.*, 2005; *Lay et al.*, 2006; *van der Hilst et al.*, 2007], and come to estimates of around 15 TW; however, areas where postperovskite is present tend to be colder and hence have a higher heat flux than the global average, so extrapolating the heat flux in these areas to the entire CMB will result in an overestimate. In our present models we obtain present-day CMB heat flows of around 9 to 10 TW, which seems reasonable: regions containing cold anomalies due to subducting slabs would have larger CMB heat flux [*Buffett*, 2007], and it would be good to study regional variations in more detail.

[25] Recently, several studies [*Yamazaki et al.*, 2006; *Yoshino and Yamazaki*, 2007; *Ammann et al.*, 2008; *Tosi et al.*, 2009] have indicated that postperovskite may have a lower viscosity than perovskite [*Yamazaki and Karato*, 2001; *Ammann et al.*, 2008], the dominant lower mantle phase. This may cause some dynamical effects that will need to be investigated.

4.3. Potassium in the Core

[26] The amount of radioactive potassium in the core is still an open issue because high-pressure experiments are difficult: one estimate of the concentration of radioactive potassium in the core is from 50 to 250 ppm [*Gessmann and Wood*, 2002; *Murthy et al.*, 2003; *Bouhifd et al.*, 2007]. Simple parameterized thermal evolution calculations suggest that the amount of the radioactive potassium could be around O(100 ppm) to O(1000 ppm) [*Labrosse*, 2003; *Roberts et al.*, 2003; *Nimmo et al.*, 2004]. Our previous study [*Nakagawa and Tackley*, 2005a] suggested that a successful evolution could be obtained with an amount of radioactive potassium in the core of O(100) ppm or less. However, our present calculations including a higher initial CMB temperature, the postperovskite phase transition, spherical geometry and an appropriate amount of MORB component in pyrolite suggest that a range of 400 ppm to 800 ppm is needed to match observational constraints, which is consistent with simple thermal evolution calculations. Parameterized models by *Davies* [2007] that explore the range of uncertainties in core thermal conductivity and other parameters obtain some successful evolution scenarios with no potassium in the core, but the mantle is parameterized rather than calculated directly. If partial melt exists near the CMB, perhaps in a global layer, then the concentration of heat-producing elements into this melt would have an important effect on thermal evolution [*Labrosse et al.*, 2007] and may reduce the required K concentration in the core. These issues require further study.

4.4. Summary and Future Directions

[27] The main points are as follows:

[28] 1. The final state of the system is only weakly dependent on initial CMB temperature, unless the CMB becomes blanketed by a global layer of dense material. Instead it is controlled primarily by the density anomaly of MORB in the deep mantle, and secondarily by the potassium concentration in the core.

[29] 2. Obtaining a successful thermal evolution, in the sense of obtaining the correct final inner core size and maintaining a geodynamo over geological time, is helped by the accumulation of piles of dense material at the CMB (subducted MORB in the present calculations) and a reasonably high concentration of radiogenic K in the core: 400–800 ppm. With these properties, the inner core is quite young, consistent with parameterized models [*Labrosse et al.*, 2001; *Nimmo et al.*, 2004].

[30] 3. The present-day CMB heat flow is around 9 TW, which is close to our previous study. While lower than estimates based on calculating tempera-

ture gradients in regions where the postperovskite transition is seismically imaged, these tend to be areas of higher than average heat flow and thus likely overestimate the global heat flow.

[31] 4. Fully 3-D spherical cases have a very similar core evolution to cases in a 2-D spherical annulus, giving confidence in the applicability of the present results.

[32] There are some major uncertainties in the core parameterization, particularly the melting temperature of iron at the center of the Earth, for which estimates range from 5400 K to 6400 K [*Alfè*, 2009], and the thermal conductivity of the core, which [*Davies*, 2007] argues is uncertain by a factor of two. Here we do not consider the effect of lateral variations in core heat flux (which we investigated in the work by *Nakagawa and Tackley* [2008]), which might even shut off the geodynamo [e.g., *Olson and Christensen*, 2002] and can also influence the growth pattern of the inner core [*Aubert et al.*, 2008]. Regarding our mantle model, the rheological properties are not quite Earth-like: the activation enthalpy is lower than realistic and the effective yield stress of the lithosphere is a gross parameterization; both of these can affect heat transport. Furthermore the reference viscosity is a little higher than Earth-like, meaning that the reference Rayleigh number is lower than Earth-like. Thermal evolution might also be affected by the inclusion of continents [e.g., *Grigné et al.*, 2007]. All of these effects should be investigated in future studies.

Acknowledgments

[33] All numerical computations were performed on ETH's Brutus cluster administrated by Informatiksdienst of ETH Zurich. The authors thank Editor Thorsten Becker and Peter van Keken and Stephane Labrosse for constructive reviews and suggestions that improved the manuscript.

References

Alfè, D. (2009), Temperature of the inner-core boundary of the Earth: Melting of iron at high pressure from first-principle coexistence simulations, *Phys. Rev. B*, *79*, 060101, doi:10.1103/PhysRevB.79.060101.

Ammann, M. W., J. P. Brodholt, and D. P. Dobson (2008), DFT study of migration enthalpies in $MgSiO_3$ perovskite, *Phys. Chem. Miner.*, *36*, 151–158, doi:10.1007/s00269-008-0265-z.

Aubert, J., H. Amit, G. Hulot, and P. Olson (2008), Thermochemical flows couple the Earth's inner core growth to mantle heterogeneity, *Nature*, *454*, 758–761, doi:10.1038/nature07109.

Boehler, R. (2000), High-pressure experiments and the phase diagram of lower mantle and core material, *Rev. Geophys.*, *38*, 221–245, doi:10.1029/1998RG000053.

Bouhifd, M. A., L. Gautron, N. Bolfan-Casanova, V. Malavergne, T. Hammouda, D. Andrault, and A. P. Jephocat (2007), Potassium partitioning into molten iron alloys at high pressure: Implications for Earth's core, *Phys. Earth Planet. Inter.*, *160*, 22–33, doi:10.1016/j.pepi.2006.08.005.

Boyet, M., and R. W. Carlson (2005), ^{142}Nd evidence for early (>4.53 Ga) global differentiation of the silicate Earth, *Science*, *309*, 576–581, doi:10.1126/science.1113634.

Brandenburg, J. P., E. H. Hauri, P. E. van Keken, and C. J. Ballentine (2008), A multiple-system study of the geochemical evolution of the mantle with force-balanced plates and thermochemical effects, *Earth Planet. Sci. Lett.*, *276*, 1–13, doi:10.1016/j.epsl.2008.08.027.

Buffett, B. A. (2002), Estimates of heat flow in the deep mantle based on the power requirements for the geodynamo, *Geophys. Res. Lett.*, *29*(12), 1566, doi:10.1029/2001GL014649.

Buffett, B. A. (2007), A bound on heat flow below a double crossing of the perovskite-postperovskite phase transition, *Geophys. Res. Lett.*, *34*, L17302, doi:10.1029/2007GL030930.

Buffett, B. A., H. E. Huppert, J. R. Lister, and A. W. Woods (1996), On the thermal evolution of the Earth's core, *J. Geophys. Res.*, *101*, 7989–8006, doi:10.1029/95JB03539.

Christensen, U. R., and A. W. Hofmann (1994), Segregation of subducted oceanic crust In the convecting mantle, *J. Geophys. Res.*, *99*(B10), 19,867–19,884, doi:10.1029/93JB03403.

Davies, G. F. (2007), Mantle regulation of core cooling: A geodynamo without core radioactivity?, *Phys. Earth Planet. Inter.*, *160*, 215–229, doi:10.1016/j.pepi.2006.11.001.

Gait, A. D., and J. P. Lowman (2007), Time-dependence in mantle convection models featuring dynamically evolving plates, *Geophys. J. Int.*, *171*, 463–477, doi:10.1111/j.1365-246X.2007.03509.x.

Gait, A. D., J. P. Lowman, and C. W. Gable (2008), Time dependence in 3-D mantle convection models featuring evolving plates: Effect of lower mantle viscosity, *J. Geophys. Res.*, *113*, B08409, doi:10.1029/2007JB005538.

Gessmann, C. L., and B. J. Wood (2002), Potassium in the Earth's core, *Earth Planet. Sci. Lett.*, *200*, 63–78, doi:10.1016/S0012-821X(02)00593-9.

Grigné, C., S. Labrosse, and P. J. Tackley (2005), Convective heat transfer as a function of wavelength: Implications for the cooling of the Earth, *J. Geophys. Res.*, *110*, B03409, doi:10.1029/2004JB003376.

Grigné, C., S. Labrosse, and P. J. Tackley (2007), Convection under a lid of finite conductivity in wide aspect ratio models: Effect of continents on the wavelength of mantle flow, *J. Geophys. Res.*, *112*, B08403, doi:10.1029/2006JB004297.

Hernlund, J. W., and P. J. Tackley (2007), Some dynamical consequences of partial melting in Earth's deep mantle, *Phys. Earth Planet. Inter.*, *162*, 149–163, doi:10.1016/j.pepi.2007.04.005.

Hernlund, J. W., and P. J. Tackley (2008), Modeling mantle convection in the spherical annulus, *Phys. Earth Planet. Inter.*, *171*, 48–54, doi:10.1016/j.pepi.2008.07.037.

Hernlund, J. W., C. Thomas, and P. J. Tackley (2005), A doubling of the post-perovskite phase boundary and structure of the Earth's lowermost mantle, *Nature*, *434*, 882–886, doi:10.1038/nature03472.

Hirose, K. (2006), Postperovskite phase transition and its geophysical implication, *Rev. Geophys.*, *44*, RG3001, doi:10.1029/2005RG000186.

Hirose, K., N. Takafuji, N. Sata, and Y. Ohishi (2005), Phase transition and density of subducted MORB crust in the lower mantle, *Earth Planet. Sci. Lett.*, *237*, 239–251, doi:10.1016/j.epsl.2005.06.035.

Jaupart, C., S. Labrosse, and J.-C. Marescal (2007), Heat and energy in the mantle of the Earth, in *Treatise of Geophysics*, vol. 7, *Mantle Dynamics*, pp. 253–303, doi:10.1016/B978-044452748-6.00114-0, Elsevier, Amsterdam.

Kesson, S. E., J. D. F. Gerald, and J. M. Shelley (1998), Mineralogy and dynamics of a pyrolite lower mantle, *Nature*, *393*(6682), 252–255, doi:10.1038/30466.

King, S. D., C. Y. Lee, P. E. van Keken, W. Leng, S. Zhong, E. Tan, N. Tosi, and M. C. Kameyama (2010), A community benchmark for 2D Cartesian compressible convection in the Earth's mantle, *Geophys. J. Int.*, *180*, 73–87, doi:10.1111/j.1365-246X.2009.04413.x.

Labrosse, S. (2003), Thermal and magnetic evolution of the Earth's core, *Phys. Earth Planet. Inter.*, *140*, 127–143, doi:10.1016/j.pepi.2003.07.006.

Labrosse, S., J.-P. Poirier, and J.-L. Le Mouël (2001), The age of the inner core, *Earth Planet. Sci. Lett.*, *190*, 111–123, doi:10.1016/S0012-821X(01)00387-9.

Labrosse, S., J. W. Hernlund, and N. Coltice (2007), A crystallizing dense magma ocean at the base of the Earth's mantle, *Nature*, *450*, 866–869, doi:10.1038/nature06355.

Lay, T., J. Hernlund, E. J. Garnero, and M. S. Thorne (2006), A post-perovskite lens and D″ heat flux beneath the central Pacific, *Science*, *314*, 1272–1276, doi:10.1126/science.1133280.

Leng, W., and S. Zhong (2008), Viscous heating, adiabatic heating and energetic consistency in compressible mantle convection, *Geophys. J. Int.*, *173*, 693–702, doi:10.1111/j.1365-246X.2008.03745.x.

Lister, J. R. (2003), Expression for the dissipation driven by convection in the Earth's core, *Phys. Earth Planet. Inter.*, *140*, 145–158, doi:10.1016/j.pepi.2003.07.007.

Lithgow-Bertelloni, C., M. A. Richards, Y. Ricard, R. J. O'Connell, and D. C. Engebretson (1993), Toroidal-poloidal partitioning of plate motions since 120 Ma, *Geophys. Res. Lett.*, *20*, 375–378, doi:10.1029/93GL00168.

Murakami, M., K. Hirose, N. Sata, Y. Ohishi, and K. Karamura (2004), Phase transition of $MgSiO_3$ perovkite in the deep lower mantle, *Science*, *304*, 855–858.

Murthy, V. R., W. van Westernen, and Y. Fei (2003), Radioactive heat source in planetary cores: Experimental evidence of potassium, *Nature*, *423*, 164–165.

Nakagawa, T., and P. J. Tackley (2004a), Effects of thermo-chemical mantle convection on the thermal evolution of the Earth's core, *Earth Planet. Sci. Lett.*, *220*, 107–119, doi:10.1016/S0012-821X(04)00055-X.

Nakagawa, T., and P. J. Tackley (2004b), Effects of perovskite-post perovskite phase change near core-mantle boundary in compressible mantle convection, *Geophys. Res. Lett.*, *31*, L16611, doi:10.1029/2004GL020648.

Nakagawa, T., and P. J. Tackley (2005a), Deep mantle heat flow and thermal evolution of the Earth's core in thermo-chemical multiphase models of mantle convection, *Geochem. Geophys. Geosyst.*, *6*, Q08003, doi:10.1029/2005GC000967.

Nakagawa, T., and P. J. Tackley (2005b), The interaction between the post-perovskite phase change and a thermo-chemical boundary layer near the core-mantle boundary, *Earth Planet. Sci. Lett.*, *238*, 204–216, doi:10.1016/j.epsl.2005.06.048.

Nakagawa, T., and P. J. Tackley (2006), Three-dimensional structures and dynamics in the deep mantle: Effects of post-perovskite phase change and deep mantle layering, *Geophys. Res. Lett.*, *33*, L12S11, doi:10.1029/2006GL025719.

Nakagawa, T., and P. J. Tackley (2008), Lateral variations in CMB heat flux and deep mantle seismic velocity caused by a thermal-chemical-phase boundary layer in 3D spherical convection, *Earth Planet. Sci. Lett.*, *271*, 348–358, doi:10.1016/j.epsl.2008.04.013.

Nimmo, F., G. D. Price, J. Brodholt, and D. Gubbins (2004), The influence of potassium on core and geodynamo evolution, *Geophys. J. Int.*, *156*, 363–376, doi:10.1111/j.1365-246X.2003.02157.x.

Oganov, A. R., and S. Ono (2004), Theoretical and experimental evidence for a post-perovskite phase of $MgSiO_3$ in Earth's D″ layer, *Nature*, *430*(6998), 445–448, doi:10.1038/nature02701.

Ohta, K., K. Hirose, T. Lay, N. Sata, and Y. Ohishi (2008), Phase transition in pyrolite and MORB at lowermost mantle convections: Implications for a MORB-rich pile above the core-mantle boundary, *Earth Planet. Sci. Lett.*, *267*, 107–117, doi:10.1016/j.epsl.2007.11.037.

Olson, P., and U. R. Christensen (2002), The time averaged magnetic field in numerical dynamos with nonuniform boundary heat flow, *Geophys. J. Int.*, *151*, 809–823, doi:10.1046/j.1365-246X.2002.01818.x.

Ono, S., E. Ito, and T. Katsura (2001), Mineralogy of subducted basaltic crust (MORB) from 25 to 37 GPa, and chemical heterogeneity of the lower mantle, *Earth Planet. Sci. Lett.*, *190*(1–2), 57–63, doi:10.1016/S0012-821X(01)00375-2.

Roberts, P. H., C. A. Jones, and A. R. Calderwood (2003), Energy fluxes and ohmic dissipation in the Earth's core, in *Earth's Core and Lower Mantle*, *The Fluid Mech. of Astrophys. and Geophys.*, vol. 11, edited by C. A. Jones, A. M. Soward, and K. Zhang, pp. 123–157, Taylor and Francis, London.

Schubert, G. (1979), Subsolidus convection in the mantles of terrestrial planets, *Annu. Rev. Earth Planet. Sci.*, *7*, 289–342, doi:10.1146/annurev.ea.07.050179.001445.

Sharpe, H. N., and W. R. Peltier (1978), Parameterized mantle convection and the Earth's thermal history, *Geophys. Res. Lett.*, *5*, 737–744, doi:10.1029/GL005i009p00737.

Solomatov, V. S. (2000), Fluid dynamics of a terrestrial magma ocean, in *Origin of the Earth and Moon*, edited by R. M. Canup and K. Righter, pp. 323–338, Univ. of Ariz. Press, Tucson.

Stevenson, D. J. (1990), Fluid dynamics of core formation, in *Origin of the Earth*, edited by H. E. Newsom and J. H. Jones, pp. 231–249, Oxford Univ. Press, New York.

Stixrude, L., and B. Karki (2005), Structure and freezing of $MgSiO_3$ liquid in Earth's lower mantle, *Science*, *310*, 297–299, doi:10.1126/science.1116952.

Tackley, P. J. (2008), Modelling compressible mantle convection with large viscosity contrasts in a three-dimensional spherical shell using the yin-yang grid, *Phys. Earth Planet. Inter.*, *171*, 7–18, doi:10.1016/j.pepi.2008.08.005.

Tackley, P. J., T. Nakagawa, and J. W. Hernlund (2007), Influence of the post-perovskite transition on thermal and thermo-chemical mantle convection, in *Post-Perovskite: The Last Mantle Phase Transition*, *Geophys. Monogr. Ser.*, vol. 174, edited by K. Hirose et al., pp. 229–248, AGU, Washington, D. C.

Tosi, N., O. Cadek, Z. Martinec, D. A. Yuen, and G. Kaufmann (2009), Is the long-wavelength geoid sensitive to the present of postperovskite above the core-mantle boundary?, *Geophys. Res. Lett.*, *36*, L05303, doi:10.1029/2008GL036902.

van der Hilst, R. D., W. V. de Hoop, P. Wang, S.-H. Shim, P. Ma, and L. Tenorio (2007), Seismostratigraphy and thermal structure of Earth's core-mantle boundary region, *Science*, *315*, 1813–1817, doi:10.1126/science.1137867.

van Keken, P. E. (2001), Cylindrical scaling for dynamical cooling model of the Earth, *Phys. Earth Planet. Inter.*, *124*, 119–130, doi:10.1016/S0031-9201(01)00195-9.

Weidner, D. J., and Y. Wang (1998), Chemical and Clapeyron-induced buoyancy at the 660 km discontinuity, *J. Geophys. Res.*, *103*, 7431–7441, doi:10.1029/97JB03511.

Williams, Q., and E. J. Garnero (1996), Seismic evidence for partial melt at the base of the Earth's mantle, *Science*, *273*, 1528–1530, doi:10.1126/science.273.5281.1528.

Williams, Q., J. S. Revenaugh, and E. J. Garnero (1998), A correlation between ultra-low basal velocities in the mantle and hot spots, *Science*, *281*, 546–549, doi:10.1126/science.281.5376.546.

Xu, W. B., C. Lithgow-Bertelloni, L. Stixrude, and J. Ritsema (2008), The effect of bulk composition and temperature on mantle seismic structure, *Earth Planet. Sci. Lett.*, *275*, 70–79, doi:10.1016/j.epsl.2008.08.012.

Yamazaki, D., and S. Karato (2001), Some mineral physics constraints on the rheology and geothermal structure of Earth's lower mantle, *Am. Mineral.*, *86*, 385–391.

Yamazaki, D., T. Yoshino, H. Ohfuji, J. Ando, and A. Yonea (2006), Origin of seismic anisotropy in the D″ layer inferred from shear deformation experiments on post-perovskite phase, *Earth Planet. Sci. Lett.*, *252*, 372–378, doi:10.1016/j.epsl.2006.10.004.

Yoshino, T., and D. Yamazaki (2007), Grain growth kinetics of $CaIrO_3$ perovskite and post-perovskite with implications for rheology of D″ layer, *Earth Planet. Sci. Lett.*, *255*, 485–493, doi:10.1016/j.epsl.2007.01.010.